CivilEng

MDPI

Article

Assessing Landslide Susceptibility in the Northern Stretch of Arun Tectonic Window, Nepal

Diwakar KC [1], Harish Dangi [2] and Liangbo Hu [1,*]

[1] Department of Civil and Environmental Engineering, University of Toledo, Toledo, OH 43606, USA; diwakar.kc@rockets.utoledo.edu
[2] NEA Engineering Company Limited, Trade Tower, Thapathali, Kathmandu 44600, Nepal; harishhappy27@gmail.com
* Correspondence: liangbo.hu@utoledo.edu

Abstract: The northern stretch of the Arun watershed in East Nepal is dominated by steep slopes and rugged topography and experiences extensive landslides each year. Reliable landslide susceptibility assessment can potentially be an important tool for risk evaluation and mitigation in the Himalayas. The present study explores two GIS-based bivariate statistical methods, the weight of evidence method and the frequency ratio method to assess the landslide susceptibility of the study area. Seven major variables including slope angle, slope aspect, slope shape, geology, stream proximity, stream power index and land use were examined as the major contributing factors to landslide occurrences in the assessment. The landslide susceptibility map produced from these two methods are characterized by four zones of very low, low, moderate and high susceptibility. The landslide percentage of each zone turns out to be consistent with the order of its susceptibility. The results suggest that the weight of evidence method is more sensitive to the spatial variation of relevant factors; both methods produced fairly reliable results, as confirmed by a success rate of 75% for the weight of evidence method and 71% for the frequency ratio method. The present study demonstrates that the quantitative assessment methods explored may have a promising potential for landslide assessment and prediction in the Himalayas.

Keywords: landslide; weight of evidence; frequency ratio; susceptibility; topography

Citation: KC, D.; Dangi, H.; Hu, L. Assessing Landslide Susceptibility in the Northern Stretch of Arun Tectonic Window, Nepal. *CivilEng* **2022**, *3*, 525–540. https://doi.org/10.3390/civileng3020031

Academic Editor: Angelo Luongo

Received: 29 April 2022
Accepted: 28 May 2022
Published: 13 June 2022

1. Introduction

Landslides are a prominent geohazard that pose a considerable threat to safety, infrastructure and environments. Landslides can be defined as the outward and downward movement of rock, earth or debris material under the action of gravity [1]. Worldwide landslides account for 17% of all casualties caused by natural hazards [2]. The weak, young Himalayas of south Asia are a region especially susceptible to landslides [3–7]. In Nepal, from the Siwalik Hills to higher Himalayas, its distinct topography, geology and geomorphology render a large part of the country inevitably vulnerable to geological hazards of various gravity-driven mass movements, potentially facilitated by seasonal rainfall, seismic movements and human activities. Every year, a significant loss in lives and properties occurs in this country, and it is imperative to develop proper hazard prediction and mitigation strategies [8].

Conventional engineering practice is primarily focused on the evaluation of the stability of individual natural or man-made slopes. In the broader context of hazard mitigation, landslide susceptibility must be assessed in the field scale to offer meaningful guidance for reducing landslide impacts. An effective method to mitigate the risk is to develop a landslide susceptibility map [9–11] for the region under investigation, which is capable of assisting the decision-making process related to human settlements and infrastructures development when highly vulnerable areas should be avoided. Traditional civil engineering analysis must be enhanced and expanded by various new approaches or techniques

with the consideration of a variety of key geological and environmental factors in order to reliably develop such assessment tools. The geographic information system (GIS) has been widely employed to generate, manage and analyze geographic data around the world, including the prediction of possible landslide hazards. Various GIS-based techniques have been explored [12,13], such as Fuzzy k-Means Classification and Bayesian Approach [14–16], logistic regression method [17–21], weight of evidence method {[10,22–25], artificial neural network method [26–28] and frequency ratio method [29,30]. A number of studies have emerged in recent years by focusing on landslide susceptibility in Nepal and around the Himalayas [5,10,29,31–35]. However, the northeastern part of Nepal has not received much interest and its landslide susceptibility has yet to be extensively explored. This region features the Lesser Himalayan Arun Tectonic Window of the Main Central Thrust zone. The northern stretch of Arun watershed in the East Nepal is dominated by steep slopes, deep river valleys, varying topography, geological structures and high gradient streams along with intense seasonal rainfall, due to which it experiences extensive landslides each year. In the present study, a number of key factors contributing to landslides in this area are discussed and incorporated into the relevant mathematical analysis. Two methods, the weight of evidence method and the frequency ratio method are explored to assess the landslide susceptibility in this area. The landslide susceptibility maps are developed based on field records of landslide events; the results of these two methods are compared and assessed.

2. Study Area

The study area in the present study is in the Sankhuwasabha District of Eastern Nepal (Figure 1), primarily focusing on the area around the Arun River. The Arun River is the major river in the study area; it flows through Nepal as part of the Sapta Koshi river system. It originates from Tibet, China, and flows south across Sankhuwasabha District, forming one of the world's deepest valleys. Many perennial streams and ephemeral channels merge into this river dendritically from the upper slope. The present study is focused on the major watershed in the northern stretch of the river. Every year, the study area experiences numerous landslides, debris flows, gully erosion, and soil slides due to its high intensity rainfall. There are also some rock falls in many locations due to their steep hill slopes where rock properties and joint orientations may also play an important role. Figure 2 shows some images of the landslides in this mountainous region.

From the geological perspective, the study area is located within one of the tectonic windows of Nepal Himalayas, i.e, the Arun Tectonic Window, which is developed in transversely folded higher Himalayan antiformal culmination [36] and consists of lesser Himalayan rock sequence surrounded by the higher Himalayan thrust sheet [37]. The uneven or rugged topography of the area is due to the presence of rocks with varying grade of metamorphism and competency: banded or augen-shaped migmatitic gneiss, followed by mica schist, quartzite and calc-schist containing higher Himalayan sequences over and around the window. Toward the top of the window, the grade of metamorphism becomes expectedly higher and indiscernibly passes into the overlying higher Himalayan sequence [36]. The study area is bounded by slope angles ranging from 0 to approximately 83°, and its elevation ranges from about 1630 to 4445 m. There are four seasons with temperate climate and polar tundra climate. Rain is the most common type of precipitation with seasonal snowfall.

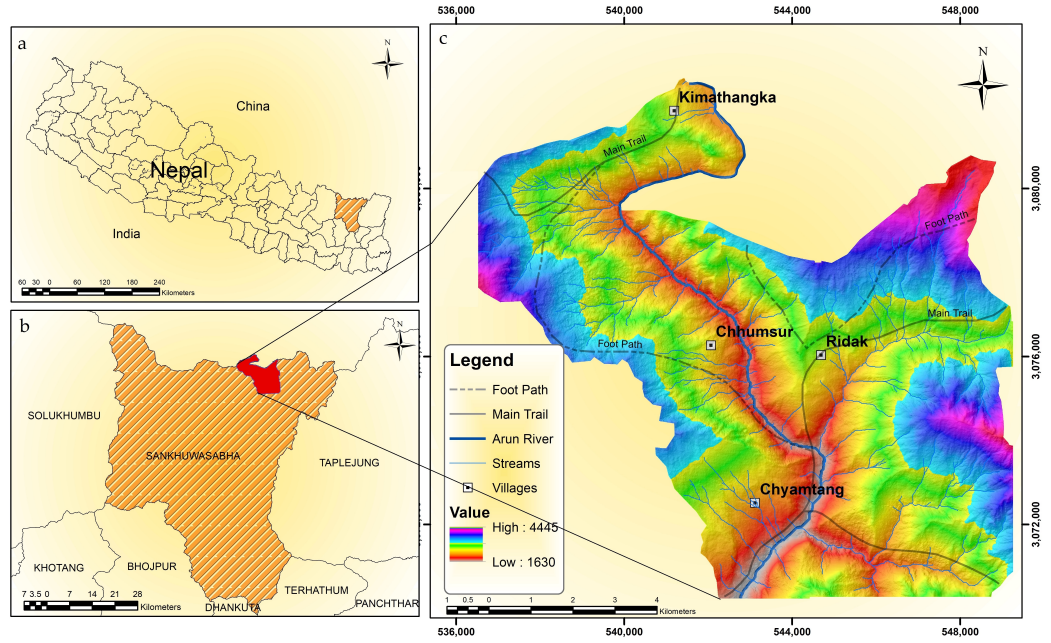

Figure 1. (**a**) Sankhuwasabha district in Nepal around neighboring countries. (**b**) Location of the study area in Sankhuwasabha District and bordering districts of Nepal. (**c**) The Arun River and many streams in the study area.

Figure 2. Sample photos of some landslides locations in the study area. The image on the right-handed side highlights three landslide slip surfaces; the two images on the left-handed side show a close-up view of the sliding surface and debris material where the loss of vegetation is evident.

3. Method

The geographic data of the study area were retrieved from available databases for the numerical analysis of landslide susceptibility. The present study examined seven major factors that are widely believed to be responsible for landslide occurrence in the field scale,

i.e., slope angle, slope aspect, slope shape, geology, stream proximity, stream power index and land use; each of them is considered in landslide susceptibility modeling.

3.1. Data Acquisition and Processing

The digital elevation model (DEM) of the study area is used in the present study. High resolution terrain-corrected DEM available from the Alaska Satellite Facility [38] is retrieved and processed for the present analysis; its resolution is 5 m by 5 m per pixel. The landslide events are identified through a field survey that thoroughly examined the entire study area for any traces of landslides; any significant trace of sliding surfaces or debris materials is considered as a landslide location. The investigation eventually revealed 74 landslides in the study area. The location and area of each landslide are typically represented by a polygon recorded using the Google Earth computer program, which is subsequently transferred to GIS for further analysis. QGIS and ArcGIS 10.7 (ESRI, USA) are used in the present study. Figure 3 shows the locations of these landslides recorded in the landslide inventory map, which also contains elevation information. The total landslide area is 0.2726 km^2, covering 0.2946% of the total study area. Some of these landslides pose potential threats to adjacent villages or roads, for which their locations are also shown in Figure 3.

Quantitative information of the five investigated factors of the study area, i.e., slope angle, slope aspect, slope shape, stream proximity and stream power index, is readily determined in the GIS tool based on the DEM retrieved. Two additional factors are explored as well, and the map of geology was prepared from field exploration and from data obtained from the Department of Mines and Geology of Nepal; a land-use map was prepared using survey data provided by the Department of Survey of Nepal.

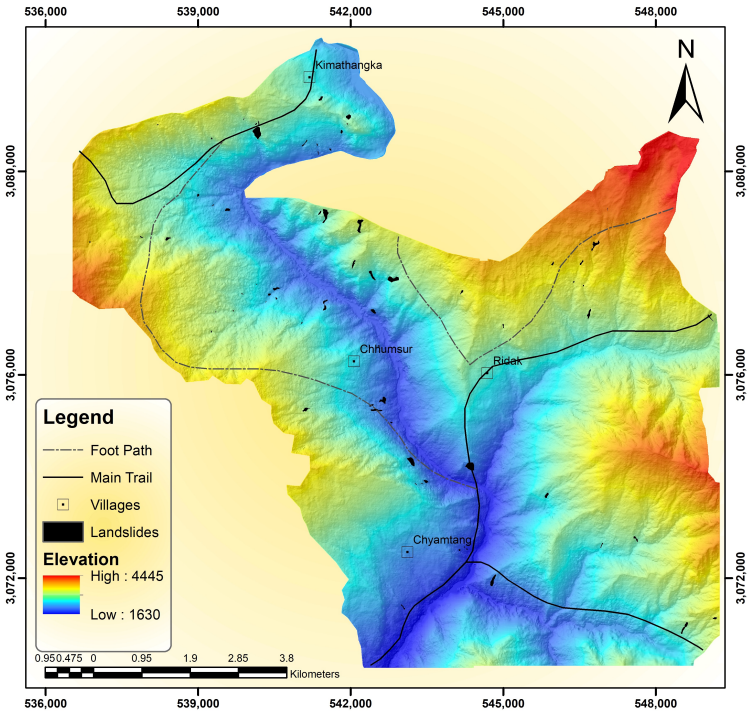

Figure 3. Elevation and landslide inventory map of the study area; each area marked in black indicates the location of the landslide.

3.2. Landslide Susceptibility Modeling

The approach adopted in the present study for landslide susceptibility modeling is based on the site's characteristics, with an aim to develop a susceptibility map of the entire study area. Two methods are explored, the weight of evidence method and the frequency

ratio method. The basis of quantitative susceptibility assessment is the site condition that is specifically characterized for each influencing factor.

For each factor, the entire domain of the study area is categorized into several classes depending on the numeric values or qualitative attributes of the factor. For example, for the first considered factor in the present study, the slope angle is categorized into seven classes: (1) 0∼15°; (2) 15°∼25°; (3) 25°∼35°; (4) 35°∼45°; (5) 45°∼55°; (6) 55°∼65°; (7) above 65°. On the other hand, the stream power index is categorized into three classes: (1) low erosion; (2) high erosion; (3) very high erosion. The details of each of the seven factors explored in the present study can be found in Section 4. Hence, each point, i.e., each pixel of the map, is characterized by seven "attributes", each of which represents one of the classes for each considered factor and is used for the mathematical modeling of landslide susceptibility.

Weight of Evidence Method

The weight of evidence (WoE) method is based on a bivariate statistical approach and is represented in a log-linear form of the Bayesian probability model that is used to estimate the relative importance of evidence. The detail on the mathematical model of the WoE method can be found in the early work of Bonham-Carter et al. [39]. In the present study, only the essential key concepts involved are briefly discussed.

For each factor, as each point (i.e., pixel) of the map is associated with a class F, the weight for the presence of this specific class, W^+, and the weight for the absence of this specific class, W^-, can be calculated as follows.

$$W^+ = \ln \frac{P(F|L)}{P(F|\bar{L})} \tag{1}$$

$$W^- = \ln \frac{P(\bar{F}|L)}{P(\bar{F}|\bar{L})} \tag{2}$$

In the above and following equations, P is the probability; the symbol L represents the presence of landslides, while $\bar{L}$ the absence of landslides; F and $\bar{F}$ represent the presence and absence of the specific class (of a factor), respectively. Therefore, $P(F|L)$ represents the probability of the specific class under the presence of a landslide, and $P(F|\bar{L})$ represents the probability of the specific class in the absence of landslide. Both probabilities can be readily calculated using the pixel numbers in the distribution map $P(F|L) = N(F|L)/N(L)$; $N(F|L)$ is the number of pixels of landslide in class F, and $N(L)$ is the total number of pixels of landslides on the map. Similarly, it can be established that $P(F|\bar{L}) = N(F|\bar{L})/N(\bar{L})$, $N(F|\bar{L})$ is the number of pixels of non-landslide in the class F and $N(\bar{L})$ is the total number of pixels of non-landslide on the map.

The weight for the absence of specific class, W^-, in Equation (2) can be calculated in a similar manner. Here, $P(\bar{F}|L)$ represents the probability of absence of the specific class F under the presence of landslide, and $P(\bar{F}|\bar{L})$ represents the probability of absence of the specific class F in the absence of landslide. Both probabilities can be readily calculated as well; $P(\bar{F}|L) = N(\bar{F}|L)/N(L)$; $N(\bar{F}|L)$ is the number of pixels of landslide in all the classes other than F; $P(F|\bar{L}) = N(F|\bar{L})/N(\bar{L})$, $N(\bar{F}|\bar{L})$ is the number of pixels of non-landslide in all the classes other than F.

The difference between the two weights is known as the weight contrast, C.

$$C = W^+ - W^- \tag{3}$$

The magnitude of contrast reflects the overall spatial correlation between the specific class of the factor and the landslides [23]. A positive value indicates a spatial association while a negative one indicates a lack of spatial association. This value is usually standardized by dividing C by its standard deviation, $S(C)$, i.e., the value of $C/S(C)$ offers as a measure of the significance of the spatial correlation [40].

The calculation of the standardized contrast is performed for each factor, and the sum of all contrasts yields the overall value of the susceptibility index for each point (each pixel) on the map.

3.3. Frequency Ratio Method

The frequency ratio method is one of the simplest methods for landslide susceptibility mapping and has been widely applied in many case studies [30,41–44]. The frequency ratio is defined as the ratio of the probability of an occurrence to the probability of a non-occurrence [40], for any given set of attributes. A low-value frequency ratio means a weak relationship between the occurrence of the landslide and the given factor's attribute [44].

Similarly to the weight of evidence method discussed above, in this method, the overall landslide susceptibility index is based on each frequency ratio, which corresponds to each influencing factor considered in the present study. For each factor, the frequency ratio can be estimated as the ratio of the percentage of landslide in the specific class to the percentage of the specific class, described as in the following equation:

$$FR = \ln \frac{L_c}{A_c} \tag{4}$$

where L_c represents the percentage of landslide in the specific class of the considered factor, and it can be calculated via $L_c = N(F|L)/N(L) \times 100\%$ using the number of pixels of landslide in the class F, $N(F|L)$ and the total number of pixels of landslides on the map, $N(L)$, as already defined in the preceding section. A_c represents the percentage of the specific class F of the entire study area; it can be calculated via $A_c = N(F)/N_t \times 100\%$ based on the number of pixels of the specific class F, $N(F)$ and the total number of pixels of entire study area on the map, N_t.

Gyawali et al. [45] developed a series of subsequent operations to improve this method by introducing the concept of relative frequency to account for weights of different factors. These modifications are also used in the present study to yield the final relative frequency ratio for each of the seven considered factors; and eventually the sum of these seven ratios provides the landslide susceptibility index.

4. Results

In the present study seven key factors that typically play a crucial role in landslides are considered in the susceptibility assessment. These factors and their distributions are discussed in Section 4.1. Subsequently, the modeling results of the susceptibility assessment based on the two methods discussed in the preceding section are presented in Section 4.2.

4.1. Influencing Factors

4.1.1. Slope Angle

The susceptibility of landslides is directly associated with their slopes. Hence, the slope is a critical factor for landslide susceptibility assessment. The slope angle in the study area ranges from 0 to 83°. The slope, typically characterized in an angle, is classified into seven different classes: (1) 0∼15°; (2) 15°∼25°; (3) 25°∼35°; (4) 35°∼45°; (5) 45°∼55°; (6) 55°∼65° and (7) above 65°. The total numbers of pixels from Class (1) to (7) are 202,156, 563,158, 1,019,975, 993,193, 591,787, 258,830 and 71,924, which correspond to the area percentage of 5.46%, 15.22%, 27.56%, 26.84%, 15.99%, 6.99% and 1.94%, respectively. The distribution of landslides in slope map is shown in Figure 4. Evidently, the slope angle of 25∼35° is the most prominent one with the highest percentage of land area, while the very steep slopes above 65° are featured very modestly in the study area.

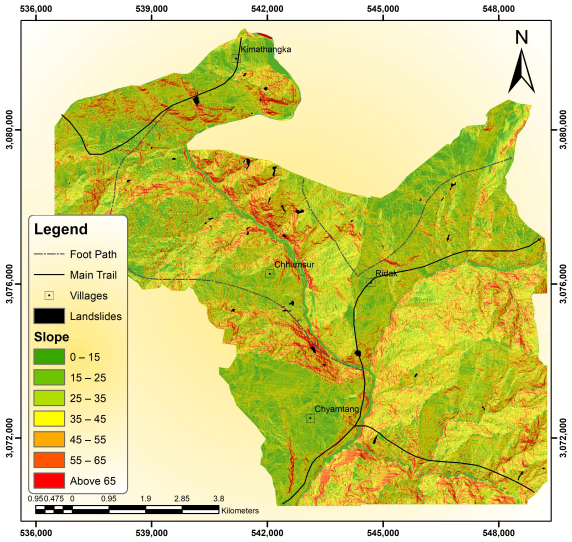

Figure 4. Distribution of slope angle in the study area.

4.1.2. Slope Aspect

Aspect is the orientation of the slope's surface, measured clockwise in degrees from 0 to 360. It is an important factor for landslides as the aspect can influence moisture and precipitation [46], which may play an important role in vegetation and rock strength. In the present study, the aspect has been classified into nine different classes (Figure 5), including (1) flat (i.e., no slope); (2) northeast (22.5°∼67.5°); (3) east (67.5°∼112.5°); (4) southeast (112.5°∼157.5°); (5) south (157.5°∼202.5°); (6) southwest (202.5°∼247.5°); (7) west (247.5°∼292.5°); (8) northwest (292.5°∼337.5°); (9) north (337.5°∼360° and 0∼22.5°). As shown in Figure 5, the largest spatial area is covered by the southeast aspect; the flat area (with no slopes) is the smallest among all classes, which demonstrates the dominance of mountainous topography.

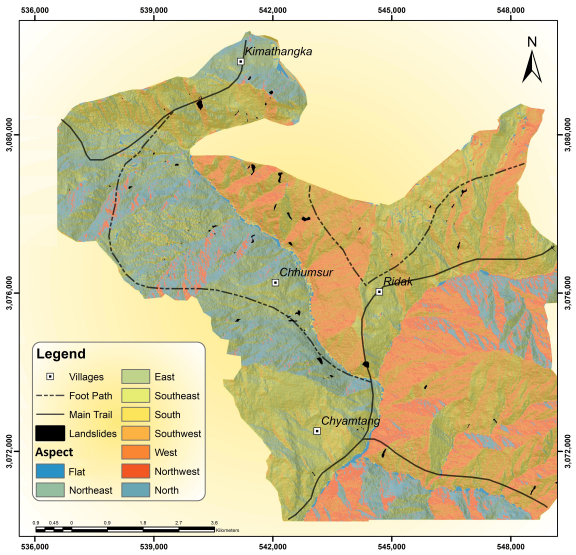

Figure 5. Distribution of slope aspect in the study area.

4.1.3. Slope Shape

Slope shape has a significant impact on slope stability in steep terrain by concentrating or dispersing surface and subsurface water in the landscape [10]. The slope shape is categorized in three spatial distribution curvatures: (1) linear; (2) concave and (3) convex. Figure 6 shows that the flat area is very small and mainly coincides with the water streams,

the areas of the concave and the convex are comparable and both are dominant in the study area.

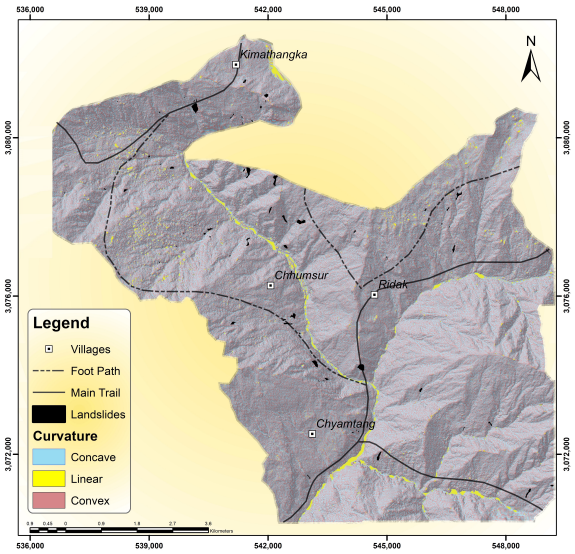

Figure 6. Distribution of slope shape in the study area.

4.1.4. Stream Proximity

The stream proximity is characterized by the distance from the location of interest to the nearest stream for which its presence has an important effect on the slope's stability. Streams can adversely affect slope stability by toe-incision or by saturating the lower part of hillslope material due to increases in water level [47,48]. The degree of saturation of slopes may also play an important role in slope stability [49,50]. In the present study, this factor is categorized in three classes: (1) 0∼100 m; (2) 100∼500 m and (3) greater than 500 m. As shown in Figure 7, the presence of close (0∼100 m) and nearby (100∼500 m) classes is very strong and is largely due to the very developed stream system in the study area.

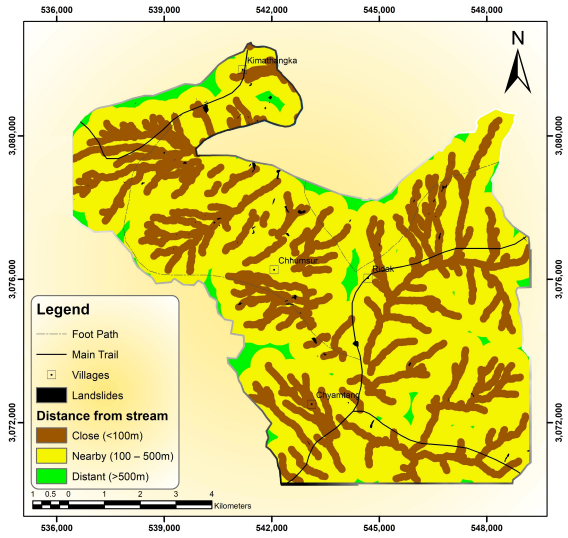

Figure 7. Distribution of stream proximity in the study area.

4.1.5. Stream Power Index

The stream power index (SPI) describes the erosive strength of the stream on the soil slope. In the present study three classes are considered: (1) low erosive; (2) high erosive

and (3) very high erosive. Figure 8 shows the distribution in the study area; most of this region is covered by areas of low erosive index.

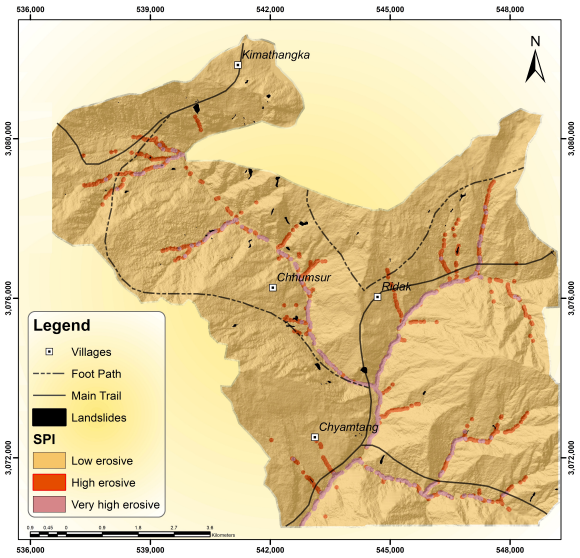

Figure 8. Distribution of stream power index in the study area.

4.1.6. Geology

The geological condition generally plays an important role in landslide susceptibility. In the present study, it refers to the lithology of various types of major rock formations in the study area, which lies within the Arun tectonic window consisting of (1) augen and banded gneiss, (2) schist and quartzite, and (3) schistose gneiss surrounded by (4) higher Himalayan crystalline rocks. In the present study, these four classes are considered, as shown in Figure 9. The Augen and banded gneiss rock is the predominant rock formation and is mainly concentrated in the western part of the study area.

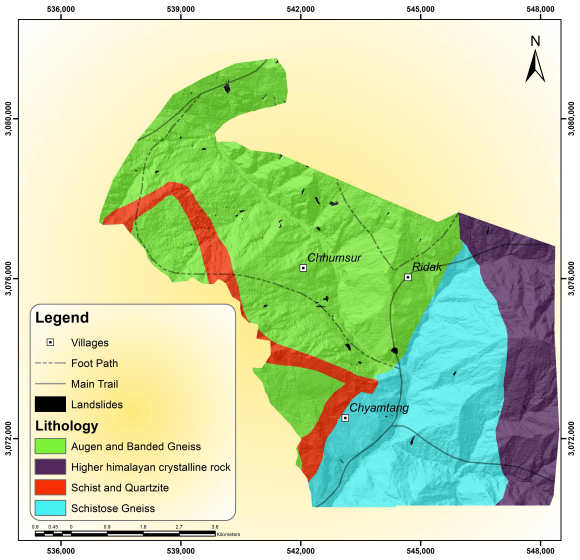

Figure 9. Distribution of rock formation in the study area.

4.1.7. Land Use

The last factor considered in the present study is associated with anthropogenic activities rather than natural environment or conditions, since the use of land may trigger or affect complex soil microbiological processes that may potentially influence slope stability. In the present study, land use is classified as five categories according to the data collected

by the Department of Survey of Nepal: (1) agricultural land; (2) barren land; (3) forest; (4) sparse vegetation; (5) water body. As shown in Figure 10, there is considerable agriculture growth in this area but it is still largely covered by sparse vegetation, which represents higher spatial coverage of bedrock rather than soil on the surface.

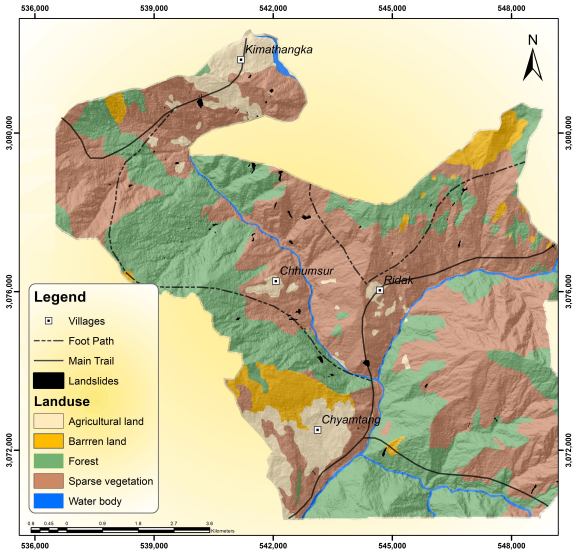

Figure 10. Distribution of land use in the study area.

4.2. Assessment Results

A landslide susceptibility map can be developed based on the weight of evidence (WoE) method or the frequency ratio (FR) method discussed in Section 3; in each method, the core step involves the calculations made for each factor. Table 1 shows the sample calculation results for the factor of slope angle in the WoE method; evidently, the rise of the slope's angle has a very positive effect on landslide susceptibility, as indicated by the increasing value of the standardized weight contrast ($C/S(C)$).

Table 1. WoE calculation results for the factor of slope angle which contains seven classes (1) 0∼15°; (2) 15°∼25°; (3) 25°∼35°; (4) 35°∼45°; (5) 45°∼55°; (6) 55°∼65°; (7) above 65°.

Slope Angle Class	Area (Pixels)	Landslides (Pixels)	W^+	W^-	C	$S(C)$	$C/S(C)$
0∼15°	202,156	60	−2.2978	0.0508	−2.3486	0.1295	−18.1398
15∼25°	563,158	533	−1.1376	0.1153	−1.2529	0.0444	−28.1940
25∼35°	1,019,975	1820	−0.5026	0.1402	−0.6429	0.0257	−25.0063
35∼45°	993,193	2970	0.0149	−0.0055	0.0204	0.0215	0.9489
45∼55°	591,787	2805	0.4773	−0.1235	0.6008	0.0220	27.3653
55∼65°	258,830	1855	0.8932	−0.1143	1.0075	0.0256	39.4025
>65°	71,924	861	1.4111	−0.0628	1.4739	0.0357	41.2706

Such calculations are repeated for other factors, and eventually the overall value of the susceptibility index for each point in the map is obtained. Typically, the susceptibility index is further classified into four zones: high, moderate, low and very low based on its value, in order to render a susceptibility map. In the present study, a common criterion [10] is adopted, i.e., to produce approximately 10% of the total area for high, 20% for moderate, 30% for low and 40% for very low susceptibility. Figure 11 shows the landslide susceptibility map based on the WoE method. Out of all recorded landslides indicated by the black color, 65% of their area turn out to lie within the moderate and high susceptible zones.

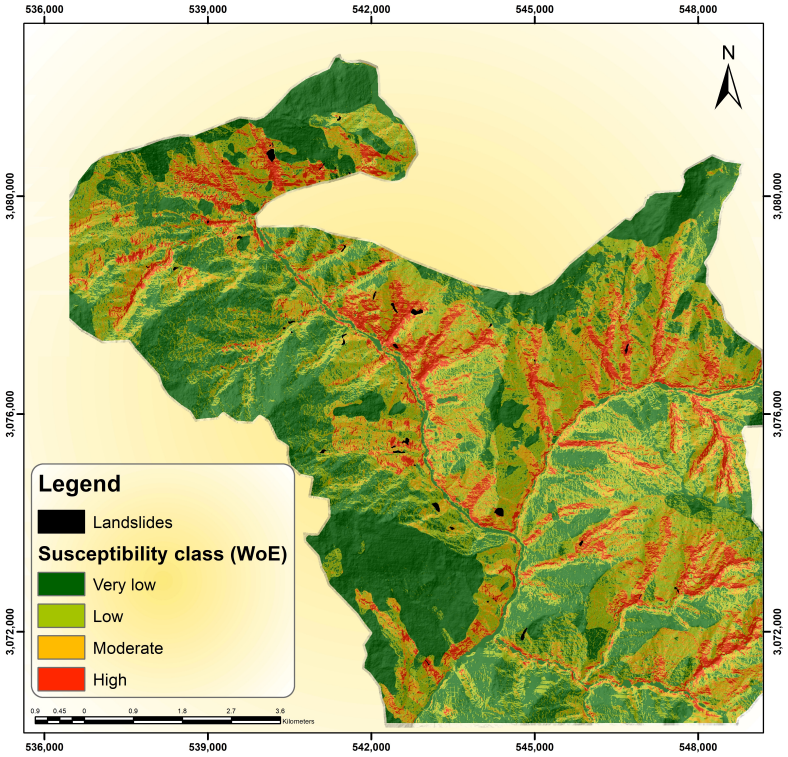

Figure 11. Landslide susceptibility map based on the weight of evidence (WoE) method

The detailed results from the weight of evidence (WoE) method are summarized in Table 2. It is noted that the area percentages are very close to but not at the precise target values of 40%, 30%, 20% and 10%, as discussed above, due to the discrete nature of the index range. The landslide density is defined as the percentage of the landslide area in each specific zone; the landslide density for high susceptibility zone is 0.89%, which gradually decreases toward very low susceptibility zone, which has a 0.06% landslide density.

Table 2. Summary of susceptibility zones and landslide density based on the weight of evidence (WoE) method.

Zone	Area		Landslides		Landslide Density
	Value (m^2)	Percentage (%)	Value (m^2)	Percentage (%)	(%)
very low	37,095,800	40.48	23,150	8.51	0.06
low	28,432,150	31.02	72,425	26.61	0.25
moderate	17,555,600	19.16	100,150	36.80	0.57
high	8,563,550	9.34	76,400	28.08	0.89

Similarly, the map based on the frequency ratio (FR) method can be also developed as shown in Figure 12. Table 3 summarizes the relevant results of different zones and landslide density. The two susceptibility maps are remarkably similar, showing that both methods are reasonably effective in producing consistent results. In the map developed from the FR method, the separation among different zones, especially between the very low and low zones, appears much clearer than the one from the WoE method; in the latter, these two zones appear more "blurred", i.e., the areas with a low susceptibility index within the range of very low or low susceptibility are intermingled. This seems to indicate that the WoE method is more sensitive to the spatial variation of relevant factors, and a lower percentage of landslides in the very low susceptibility zone indicates that the WoE may be slightly more accurate in the present study.

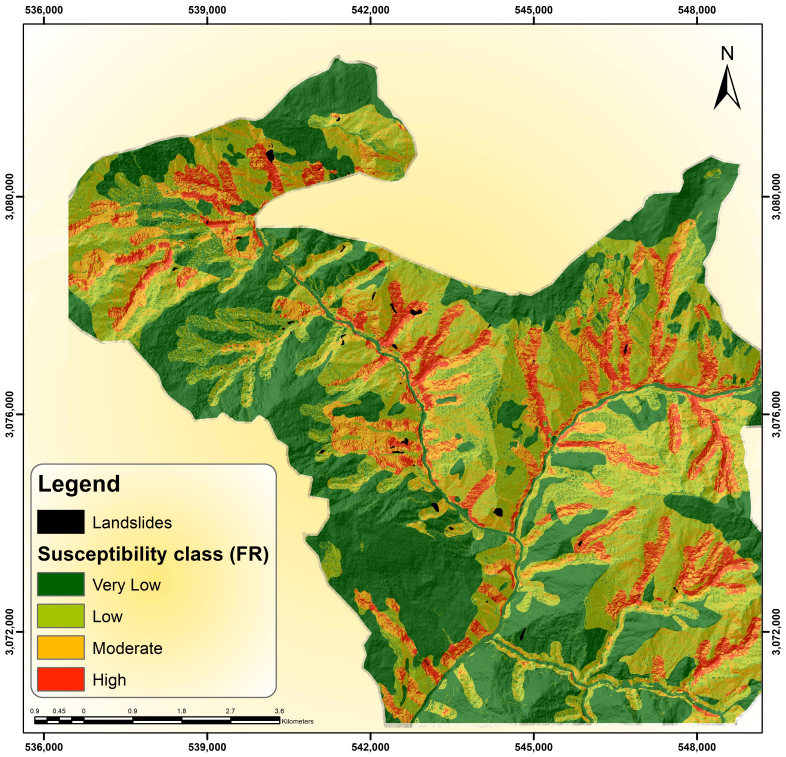

Figure 12. Landslide susceptibility map based on the frequency ratio (FR) method

Table 3. Summary of susceptibility zones and landslide density based on the frequency ratio (FR) method

Zone	Area		Landslides		Landslide Density
	Value (m^2)	Percentage (%)	Value (m^2)	Percentage (%)	(%)
very low	37,458,375	40.87	38,650	14.20	0.10
low	27,414,225	29.91	65,200	23.96	0.24
moderate	18,060,200	19.71	106,700	39.21	0.59
high	8,714,300	9.51	61,575	22.63	0.71

5. Discussion

The landslide susceptibility map can be evaluated graphically by the well-known success rating curve [10,51]. The success curves for the two methods are shown in Figure 13. On this curve, the cumulative percentage of observed landslides is plotted against the cumulative percentage of areas associated with decreasing LSI values. For example, first, the LSI values are sorted in decreasing order; then, at each select LSI value, the percentage of areas with lower LSI is calculated as the x-coordinate; it is then paired against the cumulative percentage of observed landslides (y-coordinate) that is deemed as vulnerable (due to having higher LSI), which can be calculated as the percentage of observed landslide areas in all areas with higher LSI over the total observed landslide areas. The area below this curve is considered as a quantification of success rate [51]. A perfect success rate of 100%, only possible for a straight horizontal line at $y = 100\%$ as the rating curve, implies that the landslide can only occur at the highest LSI value, which, however, is not possible or meaningful for actual field susceptibility mapping, since the landslide may occur even in areas of low susceptibility in reality. However, the area below this curve indeed offers a certain measure for how close the curve approaches perfect success. Figure 13 yields an overall success rate of 75% for the WoE method, and 71% for the FR method. These rates are generally considered fairly successful.

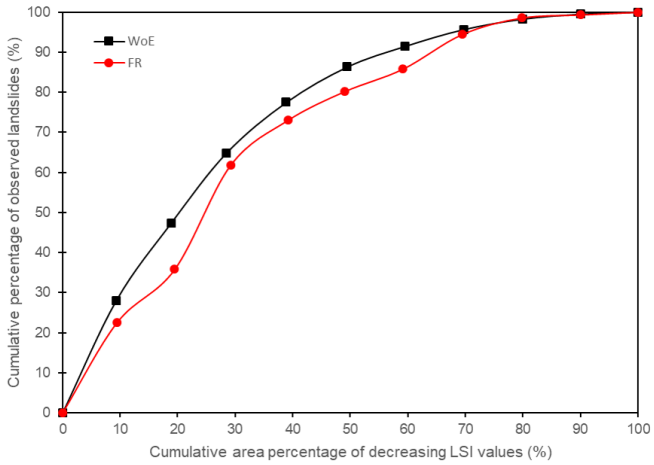

Figure 13. Success rating curves for both methods

Some other studies also reported similar success rates with the WoE method; for example, Dahal et al. [5] reported a success rate of 78% to 81% in the Nepal Himalaya; Kayastha et al. [10] reported a success rate of 79% in the Tinau watershed of Nepal. Poudyal et al. [31] obtained a success rate of 78% from the FR method and 82% from the artificial neural network (ANN) method in a case study from the Nepal Himalaya. In a case study of Izmir, Turkey, Akgun [52] used the logistic regression, frequency ratio and analytical hierarchy process (AHP) methods, which produced success rates of 81%, 76% and 71%, respectively.

It is of interest to note that there are alternative methods to measure the success rate. Vakhshoori and Zare [23] used the receiver operating characteristic (ROC) curve for their susceptibility assessments; the success rating obtained from the FR (84%) method was slightly higher than that from the WoE (83%). However, it is noted that, in the present study, the size of the sample is not very large, with only 74 landslides in the study area, and dividing these landslides into a training set and a testing set may not lead to reliable results, but this is a subject that can be explored in future studies.

6. Concluding Remarks

Landslides are a constant threat in the Himalayas, which typically feature complex arrangement of landforms with multiple geological and environmental characteristics favorable for such hazards. It is critically important to assess the landslide susceptibility and identify vulnerable areas in these mountainous regions. In the present study, an empirical approach is adopted to assess the landslide susceptibility of the northern part of Arun tectonic window in Eastern Nepal based on the records of past landslide events. Two methods are explored, including the weight of evidence method and the frequency ratio method. Seven major factors are examined, including slope angle, slope aspect, geology, slope shape, stream proximity, stream power index, and land use. In the final susceptibility maps based on the results produced from the two methods, four zones are included, very low, low, moderate and high susceptibility; the landslide density of each zone rises in this order as well, with 0.06∼0.10% in the very low susceptibility zone, gradually increasing to 0.71∼0.89% in the high susceptibility zone. The results suggest that the weight of evidence method is more sensitive to the spatial variation of relevant factors; overall, the results seem to indicate that the weight of evidence method may be slightly more accurate than the frequency ratio method in the present study. This is consistent with the success rating curves of these two methods; both yield good success rates, although the weight of evidence method has a rate of 75%, which is slightly higher than that of the frequency ratio method: 71%. The results in the present study suggest that such modeling methods explored may have a strong potential for risk assessment and prediction in the Himalayas to mitigate

losses from the landslides. Future studies may consider more relevant factors and explore high-resolution data to improve the accuracy of the susceptibility map.

Author Contributions: Conceptualization, D.K. and H.D.; methodology, D.K., H.D. and L.H.; software, D.K. and H.D.; formal analysis, D.K., H.D. and L.H.; investigation, D.K., H.D. and L.H.; resources, L.H.; data curation, D.K. and H.D.; writing—original draft preparation, D.K., H.D. and L.H.; writing—review and editing, D.K. and L.H.; visualization, D.K. and H.D.; supervision, L.H.; project administration, L.H. All authors have read and agreed to the published version of the manuscript.

Funding: This research received no external funding.

Institutional Review Board Statement: Not Applicable.

Informed Consent Statement: Not Applicable.

Data Availability Statement: Data used in the present study is contained within the article; the original DEM data are openly available from the Alaska Satellite Facility [38]

Acknowledgments: The first author (D.KC) and third author (L.Hu) wish to acknowledge the financial support provided by the University of Toledo through a Summer Research Fellowship during the preparation of this manuscript.

Conflicts of Interest: The authors declare no conflicts of interest

References

1. Cruden, D.M. A simple definition of a landslide. *Bull. Int. Assoc. Eng. Geol.* **1991**, *41*, 27–29.
2. Lacasse, S.; Nadim, F. *Landslide Risk Assessment and Mitigation Strategy*, 1st ed.; Springer: Berlin, Germany, 2009; pp. 30–35.
3. Petley, D.N.; Hearn, G.J.; Hart, A.; Rosser, N.J.; Dunning, S.A.; Oven, K.; Mitchell, W.A. Trends in landslide occurrence in Nepal. *Nat. Hazard.* **2007**, *43*, 23–44.
4. Dahal, R.K.; Hasegawa, S. Representative rainfall thresholds for landslides in the Nepal Himalaya. *Geomorphology* **2008**, *100*, 429–443.
5. Dahal, R.K.; Hasegawa, S.; Nonomura, A.; Yamanaka, M.; Dhakal, S.DEM-based deterministic landslide hazard analysis in the Lesser Himalaya of Nepal. *Georisk* **2008**, *2*, 161–178.
6. McAdoo, B.G.; Quak, M.; Gnyawali, K.R.; Adhikari, B.R.; Devkota, S.; Rajbhandari, P.L.; Sudmeier-Rieux, K. Roads and landslides in Nepal: How development affects environmental risk. *Nat. Hazards Earth Syst. Sci.* **2018**, *18*, 3203–3210.
7. Tsou, C.Y.; Chigira, M.; Higaki, D.; Sato, G.; Yagi, H.; Sato, H.P.; Wakai, A.; Dangol, V.; Amatya, S.C.; Yatagaim, A. Topographic and geologic controls on landslides induced by the 2015 Gorkha earthquake and its aftershocks: An example from the Trishuli Valley, central Nepal. *Landslides* **2018**, *15*, 953–965.
8. Dahal, B.K.; Dahal, R.K. Landslide hazard map: Tool for optimization of low-cost mitigation. *Geoenviron. Disasters* **2017**, *4*, 8.
9. Dai, F.C.; Lee, C.F.; Ngai, Y.Y. Landslide risk assessment and management: An overview. *Eng. Geol.* **2002**, *64*, 65–87.
10. Kayastha, P.; Dhital, M.R.; De Smedt, F. Landslide susceptibility mapping using the weight of evidence method in the Tinau watershed, Nepal. *Nat. Hazard.* **2012**, *63*, 479–498.
11. Forte, G.; De Falco, M.; Santangelo, N.; Santo, A. Slope stability in a multi-hazard eruption scenario (Santorini, Greece). *Geosciences*, **2019**, *9*, 412.
12. Reichenbach, P.; Rossi, M.; Malamud, B.D.; Mihir, M.; Guzzetti, F. A review of statistically-based landslide susceptibility models. *Earth Sci. Rev.* **2018**, *180*, 60–91.
13. Yan, F.; Zhang, Q.; Ye, S.; Ren, B. A novel hybrid approach for landslide susceptibility mapping integrating analytical hierarchy process and normalized frequency ratio methods with the cloud model. *Geomorphology* **2019**, *327*, 170–187.
14. Gorsevski, P.V.; Gessler, P.E.; Jankowski, P. Integrating a fuzzy k-means classification and a Bayesian approach for spatial prediction of landslide hazard. *J. Geogr. Syst.* **2003**, *5*, 223–251.
15. Kaur, H.; Gupta, S.; Parkash, S. Comparative evaluation of various approaches for landslide hazard zoning: A critical review in Indian perspectives. *Spatial Information Research* **2017**, *25*, 389–398.
16. Wang, Q.; Wang, Y.; Niu, R.; Peng, L. Integration of information theory, K-means cluster analysis and the logistic regression model for landslide susceptibility mapping in the Three Gorges Area, China. *Remote Sens.* **2017**, *9*, 938.
17. Lee, S. Application of likelihood ratio and logistic regression models to landslide susceptibility mapping using GIS. *Environ. Manag.* **2004**, *34*, 223–232.
18. Ayalew, L.; Yamagishi, H. The application of GIS-based logistic regression for landslide susceptibility mapping in the Kakuda-Yahiko Mountains, Central Japan. *Geomorphology* **2005**, *65*, 15–31.
19. Yesilnacar, E.; Topal, T.A.M.E.R. Landslide susceptibility mapping: A comparison of logistic regression and neural networks methods in a medium scale study, Hendek region (Turkey). *Eng. Geol.* **2005**, *79*, 251–266.
20. Bui, D.T.; Lofman, O.; Revhaug, I.; Dick, O. Landslide susceptibility analysis in the Hoa Binh province of Vietnam using statistical index and logistic regression. *Nat. Hazard.* **2011**, *59*, 1413–1444.

21. Yang, J.; Song, C.; Yang, Y.; Xu, C.; Guo, F.; Xie, L. New method for landslide susceptibility mapping supported by spatial logistic regression and GeoDetector: A case study of Duwen Highway Basin, Sichuan Province, China. *Geomorphology* **2019**, *324*, 62–71.
22. Ilia, I.; Tsangaratos, P. Applying weight of evidence method and sensitivity analysis to produce a landslide susceptibility map. *Landslides* **2004**, *13*, 379–397.
23. Vakhshoori, V.; Zare, M. Landslide susceptibility mapping by comparing weight of evidence, fuzzy logic, and frequency ratio methods. *Geomat. Nat. Hazards Risk* **2016**, *7*, 1731–1752.
24. Hong, H.; Ilia, I.; Tsangaratos, P.; Chen, W.; Xu, C. Applying weight of evidence method and sensitivity analysis to produce a landslide susceptibility map.A hybrid fuzzy weight of evidence method in landslide susceptibility analysis on the Wuyuan area, China. *Geomorphology* **2017**, *290*, 1–16.
25. Xie, Z.; Chen, G.; Meng, X.; Zhang, Y.; Qiao, L.; Tan, L. A comparative study of landslide susceptibility mapping using weight of evidence, logistic regression and support vector machine and evaluated by SBAS-InSAR monitoring: Zhouqu to Wudu segment in Bailong River Basin, China. *Environ. Earth Sci.* **2017**, *76*, 1–19.
26. Lee, S.; Evangelista, D.G. Earthquake-induced landslide-susceptibility mapping using an artificial neural network. *Nat. Hazards Earth Syst. Sci.* **2006**, *6*, 687–695.
27. Choi, J.; Oh, H.J.; Won J.S.; Lee, S. Validation of an artificial neural network model for landslide susceptibility mapping. *Environ. Earth Sci.* **2010**, *60*, 473–483.
28. Chen, W.; Pourghasemi, H.R.; Zhao, Z. A GIS-based comparative study of Dempster-Shafer, logistic regression and artificial neural network models for landslide susceptibility mapping. *Geocarto Int.* **2017**, *32*, 367–385.
29. Akinci, H.; Doan, S.; Kiliccedil, C.; Temiz, M.S. DProduction of landslide susceptibility map of Samsun (Turkey) City Center by using frequency ratio method. *Int. J. Phys. Sci.* **2011**, *6*, 1015–1025.
30. Park, S.; Choi, C.; Kim, B.; Kim, J. Landslide susceptibility mapping using frequency ratio, analytic hierarchy process, logistic regression, and artificial neural network methods at the Inje area, Korea. *Environ. Earth Sci.* **2013**, *68*, 1443–1464.
31. Poudyal, C.P.; Chang, C.; Oh, H.J.; Lee, S. Landslide susceptibility maps comparing frequency ratio and artificial neural networks: A case study from the Nepal Himalaya. *Environ. Earth Sci.* **2010**, *61*, 1049–1064.
32. Kayastha, P.; Dhital, M.R.; De Smedt, F. Evaluation and comparison of GIS based landslide susceptibility mapping procedures in Kulekhani watershed, Nepal. *J. Geol. Soc. India* **2013**, *81*, 219–231.
33. Bijukchhen, S.M.; Kayastha, P.; Dhital, M.R. A comparative evaluation of heuristic and bivariate statistical modelling for landslide susceptibility mappings in Ghurmi-Dhad Khola, east Nepal. *Arabian J. Geosci.* **2013**, *6*, 2727–2743.
34. Dahal, R.K. Regional-scale landslide activity and landslide susceptibility zonation in the Nepal Himalaya. *Environ. Earth Sci.* **2014**, *71*, 5145–5164.
35. Amatya, P.; Kirschbaum, D.; Stanley, T. Use of very high-resolution optical data for landslide mapping and susceptibility analysis along the Karnali highway, Nepal. *Remote Sens.* **2019**, *11*, 2284.
36. Dhital, M.R. *Geology of the Nepal Himalaya*; Springer International Publishing: Cham, Switzerland, 2015.
37. Schelling, D. The tectonostratigraphy and structure of the eastern Nepal Himalaya. *Tectonics* **1992**, *11*, 925–943.
38. Alaska Satellite Facility. Available online: https://asf.alaska.edu (accessed on 12 October 2021).
39. Bonham-Carter, G.F.; Agterberg, F.P.; Wright, D.F. Integration of geological datasets for gold exploration in Nova Scotia. *Photogramm. Eng. Remote Sens.* **1988**, *54*,1585–1592.
40. Bonham-Carter, G. F. *Geographic Information Systems for Geoscientists, Modeling with GIS*; Elsevier: Amsterdam, The Netherlands, 1994.
41. Lee, S.; Pradhan, B. Landslide hazard mapping at Selangor, Malaysia using frequency ratio and logistic regression models. *Landslides* **2007**, *4*, 33–41.
42. Jadda, M.; Shafri, H.Z.M.; Mansor, S.B.; Sharifikia, M.; Pirasteh, S. Landslide susceptibility evaluation and factor effect analysis using probabilistic-frequency ratio model. *Eur J Sci Res.* **2009**, *33*, 654–668.
43. Yilmaz, I. Landslide susceptibility mapping using frequency ratio, logistic regression, artificial neural networks and their comparison: A case study from Kat landslides (Tokat-Turkey). *Comput Geosci.* **2009**, *35*, 1125–1138.
44. Lee, S.; Talib, J.A. Probabilistic landslide susceptibility and factor effect analysis. *Environ. Geol.* **2005**, *47*, 982–990.
45. Gyawali, P.; Aryal, Y.M.; Tiwari, A.; Prajwol, K.C.; Ansari, K. Landslide Susceptibility Assessment Using Bivariate Statistical Methods: A Case Study of Gulmi District, western Nepal. *VW Eng. Int.* **2021**, *3*, 29–40.
46. Dangi, H.; Bhattarai, T.N.; Thapa, P.B. An approach of preparing earthquake induced landslide hazard map: A case study of Nuwakot District , central Nepal. *Nepal Geol. Soc.* **2019**, *58*, 153–162.
47. Gokceoglu, C.; Aksoy, H. Landslide susceptibility mapping of the slopes in the residual soils of the Mengen region (Turkey) by deterministic stability analyses and image processing techniques. *Eng. Geol.* **1996**, *44*, 147–161.
48. Kanungo, D.P.; Singh, R.; Dash, R.K. Field observations and lessons learnt from the 2018 landslide disasters in Idukki District, Kerala, India. *Curr. Sci.* **2020**, *119*, 1797.
49. Yalcin, A.; Bulut, F. Landslide susceptibility mapping using GIS and digital photogrammetric techniques: A case study from Ardesen (NE-Turkey). *Nat. Hazards* **2007**, *41*, 201–226.
50. Yalcin, A. GIS-based landslide susceptibility mapping using analytical hierarchy process and bivariate statistics in Ardesen (Turkey): Comparisons of results and confirmations. *Catena* **2008**, *72*, 1–12.
51. Van Westen, C.J.; Rengers, N.; Soeters, R. Use of geomorphological information in indirect landslide susceptibility assessment. *Nat. Hazards* **2003**, *30*, 399–419.

52. Akgun, A. A comparison of landslide susceptibility maps produced by logistic regression, multi-criteria decision, and likelihood ratio methods: A case study at Izmir, Turkey. *Landslides* **2012**, *9*, 93–106.